

DOI: 10.1002/cmdc.201402244

α -Keto Phenylamides as P1'-Extended Proteasome Inhibitors

Constantin Voss,^[a] Christoph Scholz,^[a] Sabine Knorr,^[b] Philipp Beck,^[c] Martin L. Stein,^[c] Andrea Zall,^[a] Ulrike Kuckelkorn,^[d] Peter-Michael Kloetzel,^[d] Michael Groll,^[c] Kay Hamacher,^[b] and Boris Schmidt^{*[a]}

The major challenge for proteasome inhibitor design lies in achieving high selectivity for, and activity against, the target, which requires specific interactions with the active site. Novel ligands aim to overcome off-target-related side effects such as peripheral neuropathy, which is frequently observed in cancer patients treated with the FDA-approved proteasome inhibitors bortezomib (**1**) or carfilzomib (**2**). A systematic comparison of electrophilic headgroups recently identified the class of α -keto amides as promising for next generation drug development. On the basis of crystallographic knowledge, we were able to develop a structure–activity relationship (SAR)-based approach for rational ligand design using an electronic parameter (Ham-

mett's σ) and in silico molecular modeling. This resulted in the tripeptidic α -keto phenylamide BSc4999 [(S)-3-(benzyloxycarbonyl-(S)-leucyl-(S)-leucylamino)-5-methyl-2-oxo-N-(2,4-dimethylphenyl)hexanamide, **6a**], a highly potent (IC_{50} = 38 nM), cell-permeable, and slowly reversible covalent inhibitor which targets both the primed and non-primed sites of the proteasome's substrate binding channel as a special criterion for selectivity. The improved inhibition potency and selectivity of this new α -keto phenylamide makes it a promising candidate for targeting a wider range of tumor subtypes than commercially available proteasome inhibitors and presents a new candidate for future studies.

Introduction

Intracellular protein degradation via the ubiquitin–proteasome system is crucial for protein homeostasis within eukaryotic organisms. The 26S proteasome is a sophisticated multicatalytic molecular degradation machinery consisting of a proteolytic 20S core particle (CP) surrounded by two regulatory 19S caps, which are responsible for the recognition of ubiquitin marked substrates, their unfolding, and transport to the inner CP. The 20S proteasome appears as an elongated hollow cylinder forming the multicatalytic center: four heptameric rings form a pile following an $\alpha_7\beta_7\beta_7\alpha_7$ stoichiometry.^[1] The binding channels of the proteasome active sites within the inner β -rings bear different subpockets that are essential for the specific binding of defined substrate peptides. A systematic nomenclature differenti-

ates the primed and a non-primed regions of this channel, starting from the cleavage site of a peptide substrate.^[2]

However, fluorogenic assays with eukaryotic cells revealed that each β -ring only harbors three catalytic active sites with distinct substrate preferences: β_1 cleaves after acidic residues and therefore mimics a caspase-like (CL) activity, β_2 displays trypsin-like (TL) activity, while β_5 typifies chymotrypsin-like (ChTL) activity.

The mode of action of each active site follows a uniform mechanism employing an N-terminal threonine (Thr1) hydrolyzing the substrate's scissile peptide bond by nucleophilic attack of its hydroxy group (Thr1O⁻). The N terminus (Thr1N) acts via a water molecule and coordinates the proton shuttle and cleavage of the acyl–enzyme intermediate by the release of defined oligopeptides with a length distribution between three and 25 amino acids.^[3] Due to the central role of the CP in antigen processing, cell cycle control, cell signaling, and protein quality control, this protease represents an important target in the fields of cell biology, structural biology, and medicinal chemistry. Numerous specific and nonspecific inhibitors have been developed to target proteasome activities.^[4] This led to the approval of the boronic acid bortezomib (**1**) by the US Food and Drug Administration (FDA) in 2003 and, most recently, the epoxyketone carfilzomib (**2**) for the treatment of multiple myeloma in 2012 (Figure 1).^[5]

So far, the majority of known natural or synthetic inhibitors of the proteasome addresses the non-primed site of the binding channel. However, the primed regions show significant variations amongst the active sites and thus can be used as selec-

[a] C. Voss, C. Scholz, Dr. A. Zall, Prof. Dr. B. Schmidt
Clemens Schöpf Institute for Organic Chemistry & Biochemistry
Technische Universität Darmstadt
Alarich Weiss-Str. 4-8, 64287 Darmstadt (Germany)
E-mail: schmidt_boris@t-online.de

[b] S. Knorr, Prof. Dr. K. Hamacher
Computational Biology & Simulation, Technische Universität Darmstadt
Schnittspahnstr. 10, 64287 Darmstadt (Germany)

[c] P. Beck, Dr. M. L. Stein, Prof. Dr. M. Groll
Center of Integrated Protein Science at the Department of Chemistry
Chair of Biochemistry, Technische Universität München
Lichtenbergstr. 4, 85747 Garching (Germany)

[d] Dr. U. Kuckelkorn, Prof. Dr. P.-M. Kloetzel
Institute of Biochemistry CCM, Charité Universitätsmedizin Berlin
Charitéplatz 1/Virchowweg 6, 10117 Berlin (Germany)

 Supporting information for this article is available on the WWW under <http://dx.doi.org/10.1002/cmdc.201402244>.

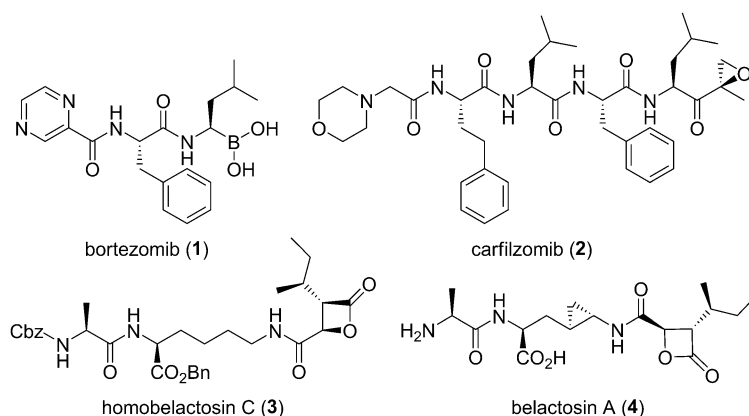


Figure 1. Structures of FDA-approved proteasome inhibitors **1** and **2**, as well as **3**, which binds to the primed site of the proteasome substrate binding channel, and its natural product counterpart **4**.

tivity criteria for structure-guided inhibitor design. As an example, the β -lactone proteasome inhibitor homobelactosin C (**3**, Figure 1) shows high β 5-selectivity by occupying the primed site of the ChTL substrate binding channel. Interestingly, this natural product displays high antitumor activity, with nanomolar IC_{50} values in human pancreoma and colon cancer cells.^[6] Crystallographic analysis of this ligand in complex with the yeast 20S proteasome identified that its high selectivity was caused by an unexpected mode of action.^[7] Thus, **3** and its natural counterpart, belactosin A (**4**, Figure 1), turned out to be promising leads for the design of new and highly selective proteasome inhibitors.^[8] Even though acyl-ester formation of the β -lactone headgroup with Thr10' follows a reversible mechanism, the ligand orientation blocks access to a water molecule, preventing deacetylation. The resulting long half-life of β -lactone-induced inhibition is similar to the activity of irreversibly binding ligands. This imposes limits for deep solid tissue penetration, restricting these inhibitors to the treatment of non-solid tumors.^[9]

Recently, the class of reversible and potent peptidic α -keto amides has been shown to exploit both the primed and the non-primed sites, thereby compensating for their moderate chemical reactivity and leading to a strong proteasome binding preference.^[10] It turned out that the α -keto phenylamide headgroup harbors a potential motif for ligand optimization, due to its unique orientation in the CP active site cavity with the terminal phenylamide moiety projecting into the primed site of the binding channel. Furthermore, it is the α -keto phenylamide residue that accounts for the ligand's inhibitory potency.

Therefore α -keto phenylamide CP inhibitors are promising candidates for preclinical studies of a wider range of tumor subtypes as currently targeted by bortezomib (**1**) and carfilzomib (**2**). This work describes the development of an inhibitor based on the α -keto phenylamide headgroup, that engages in additional primed site interactions and thus exhibits improved potency.

Results

In a previous work,^[10a] BSc2189 (**5**, Figure 2A) was identified as a promising potent proteasome inhibitor (IC_{50} : 72 nM) that exhibits high selectivity for the β 5 subunit. Diminished proteolysis in the cytosolic fraction, as well as in the protease inhibitor mixture-pretreated lysate (Complete, Roche Applied Science), confirmed inhibitory activity exclusively to the CP and distinguished it from inhibition of most cytosolic serine/aspartate proteases. X-ray data from crystallization of the compound in complex

with the yeast 20S proteasome revealed hemiacetal formation in the α -position of the phenylamide moiety, due to nucleophilic attack of the ligand α -ketone by Thr10' (Figure 2A).^[10c] The observation of the amide terminus occupying the S1' cavity of the binding channel is in accordance with a previous work from Chatterjee et al.^[10b] X-ray data revealed the ligand's primed site residue (P1') extending into the hollow inner side of the cylindrical CP. The attack by Thr10' on the ligand's "s" face enables hydrogen bond formation between the hemiacetal and Thr1N (Figure 2B). Occupation of the oxyanion hole formed by Gly47N with the terminal amide carbonyl group additionally stabilizes the ligand's orientation on the target. However, the most notable feature of **5** is its aromatic C-terminal phenylamide moiety that resides in an almost perfectly planar fashion in the S1' subpocket of the binding channel (Figure 2D). This rigidity of the P1' residue of the ligand contributes to the driving force for its high-affinity binding, as decreased degrees of freedom in the unbound state restrict the entropic penalty upon binding.

As a proof of concept, we investigated the variation in the electron density of the aromatic system by introducing substituents at the *para* position of the phenyl moiety in P1'. Both electron donating (**6b**; **6c**) and electron withdrawing groups (**6d**; **6e**) were analyzed in this study. We converted the respective anilines (**7a–d**) to formamides (**8a–d**, Scheme 1) to provide access to functionalized derivatives of **5**. N-formylation was performed according to a published catalyst- and solvent-free procedure, which was adopted for anilines **7a–d**.^[11] The subsequent conversion into isonitriles **9a–e** was followed by a dehydration step, using phosphorus oxychloride and triethylamine in dichloromethane.^[12] Subsequent conversion was done directly after a quick workup of hydrolytically labile compounds **9a–e**. The tripeptidic aldehyde Cbz-Leu-Leu-Leu-al and trifluoroacetic acid then underwent a multicomponent Passerini reaction with isonitriles **9a–e** to form α -hydroxyphenylamides **10a–e**. Oxidation with 2-iodoxybenzoic acid (IBX) provided the desired tripeptidic α -keto amides **6a–e** in moderate yields, as displayed in Scheme 1.

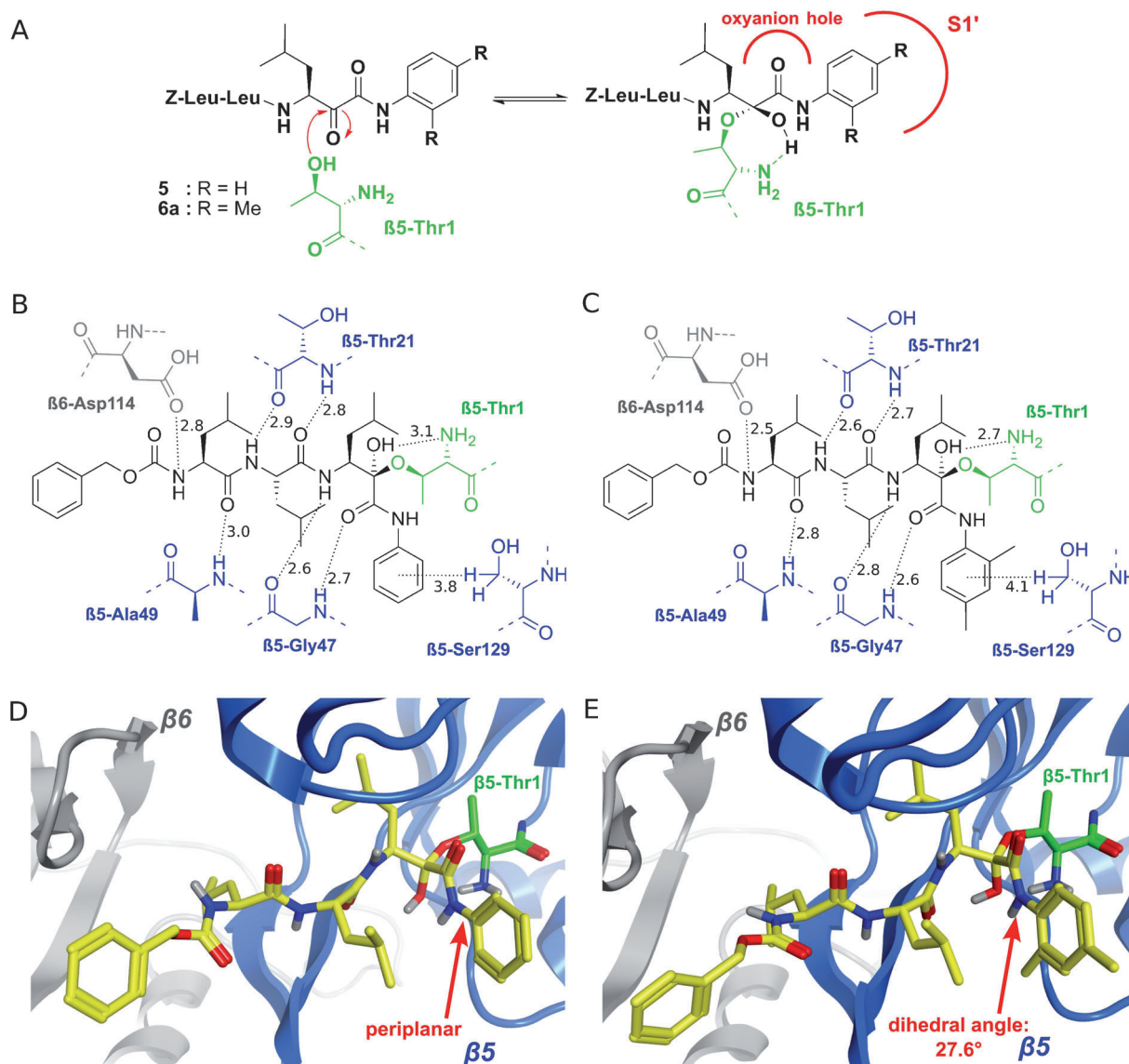
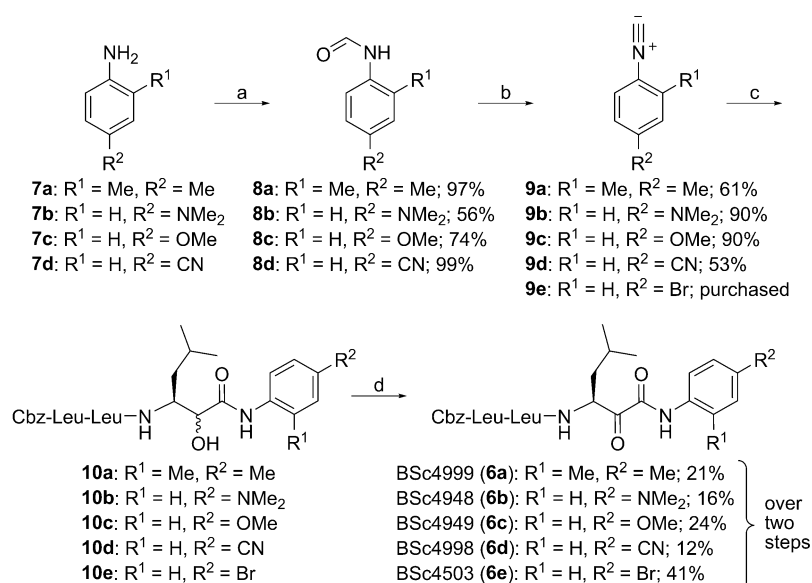


Figure 2. A) Binding mechanism of α -keto phenylamides to the β_5 subunit of the 20S proteasome. Reversible hemiacetal formation by nucleophilic attack of the catalytically active Thr 1 (green) with the ketone moiety of the inhibitor (black). B)–E) Crystal structures of BSc2189 (**5**, PDB code: 4NO8) and BSc4999 (**6a**, PDB code: 4R02) in complex with the yeast CP. B, C) 2D images show interactions as grey dashed lines between the inhibitor and relevant subpocket residues of the proteasome (blue/grey). D, E) 3D images show the ligands as stick models (yellow) and the proteasome subunits in ribbon/loop representation (blue/grey). The dihedral angles ($\angle_{\text{C}_{\text{carbonyl}}-\text{N}-\text{C}_{\text{phenyl}}-\text{C}_{\text{phenyl}}}$) of the ligand phenyl amide moieties are indicated by red arrows.

A structure–activity relationship study was established for our ensemble of initial derivatives **6b–e**, using the tabulated Hammett’s constants (σ), a parameter expressing the electronic constitution of an aromatic reaction center in dependency of the nature of a substituent at a *meta* or *para* position.^[13] Our hypothesis is that the binding process to the CP predominantly depends on the electron density of the aromatic C-termini, modified by different *para* substituents in **6b–e**. Therefore, we performed a hypothesis test in which we plotted logarithmic IC_{50} values against the respective σ constants. As a result, we identified a linear correlation supporting our hypothesis: biological data were consistent with the SAR for all *para*-substituted compounds (**6b–e**), demonstrating a loss in activity with higher σ constants (Figure 3).

Accordingly, we observed that increased electron density of the aromatic system, which is induced by electron donating substituents, resulted in a stronger double bond character of the nitrogen–phenyl bond ($\text{N}-\text{C}_{\text{phenyl}}$) and, thus, to increased rigidity. We assume this to be the major feature of an entropically favored binding process, thus corresponding to the improved biological activity. Nevertheless, all derivatives carrying functional groups in the *para* position were less active than the unsubstituted phenylamide lead (**5**). For illustration purposes, we have included **5** in Figure 3. Hence, we aimed to characterize the intermolecular forces within the primed site of the β_5 subunit. The SAR study suggested that the electron donating groups play a key role in the affinity of the inhibitor, contrary to the withdrawing groups. As the considered elec-



Scheme 1. Synthesis of target compounds **6a–e**. Reagents and conditions: a) HCO₂H, 60 °C; b) POCl₃, NEt₃, CH₂Cl₂, 0 °C; c) 1. Cbz-Leu-Leu-Leu-al, pyridine, CH₂Cl₂, –10 °C, 2. TFA, 0 °C; d) IBX, DMSO, RT. Percent yields are shown; for **6a–e**, yields were calculated over two reaction steps, as **10a–e** were not isolated.

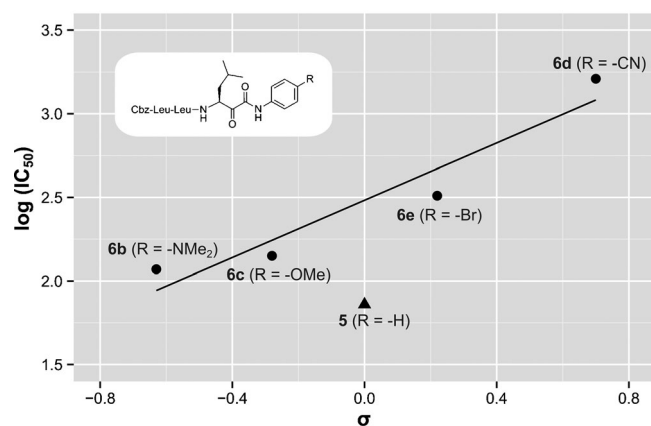


Figure 3. Plot of logarithmic IC₅₀ values of inhibitors **6b–e** against respective Hammett's constants σ (●). Note the significant linear correlation ($p \leq 0.0409$) between $\log(\text{IC}_{50})$ and σ . For illustrative purposes, we also added a single data point for **5** (▲). Significance tests were performed based on our starting hypothesis for exclusively *para*-substituted derivatives **6b–e**. Linear correlation: $\log(\text{IC}_{50}) = 0.85584\sigma + 2.48202$.

tron donating groups of **6b** and **6c** predominantly act as hydrogen bond acceptors, water molecules are coordinated by each of the ligands and cause a decrease in their binding preference by compensating for the benefit of high electron density within the aromatic system. We therefore propose that methyl groups donate electron density into the aromatic system by σ -conjugation, but they do not participate in hydrogen bonding. We performed a docking study to evaluate the most promising compound of the five possible *ortho*- and *para*-substituted methylphenylamide derivatives. Covalent docking with flexible side chains of the receptor was realized with *conflexdock* within the MOE2012.10 software.^[14] First,

a conformational database spanning different dihedral angles between the plane of the respective aromatic system and the amide moiety was generated by keeping the peptidic backbone in its "native conformation", based on the blueprint of the CP-5 X-ray structure. Next, simulations starting with iterated dihedral angles in 45° steps were carried out to determine relative energy minima, allowing us to rank the ligands according to their respective energies (see Supporting Information). The 2,4-dimethyl substitution displayed the lowest overall energy score, suggesting the synthesis of ligand **6a**. In agreement with our modeling studies, **6a** turned out to be the most potent inhibitor of the 20S proteasome within this series. Blocking the

ChTL activity in vitro resulted in an IC₅₀ value of 38 nM. Moreover, this compound is selective for the ChTL substrate binding channel, as the CL and the TL activities remained unaffected (Table 1).

Table 1. Activities of peptidic α -keto phenylamides **6a–e** against the three catalytic activities of isolated proteasomes.^[a]

Compd	IC ₅₀ [nM] ^[b]		
	ChTL (β 5)	TL (β 2)	CL (β 1)
6a	38 ± 19	> 3000	NA
6b	118 ± 40	NA	NA
6c	142 ± 95	> 9000	NA
6d	1608 ± 53	NA	NA
6e	326 ± 35	NA	NA

[a] See Scheme 1 for compound structures. [b] Data, normalized to controls, are the means of two independent experiments, each performed in triplicate ($n=2$); in vitro data for lead compound **5** (IC_{50, β 5} = 72 nM) were published previously.^[10a] NA: not affected (IC₅₀ > 10 μ M).

Crystallographic data of **6a** in complex with the yeast 20S proteasome revealed that the dimethylated aromatic system is twisted out of the amide plane, with a dihedral angle of 27.6°, in contrast with the co-planar keto amide moiety of lead **5** upon CP binding (Figure 2D,E). This conformational change is interpreted as an on-target effect due to steric and enthalpic interactions within the active site, which compensates for the electronically favored periplanar shape. Note, these findings are in agreement with our predictions, as a hindered rotation of the C_{carbonyl}–N–C_{phenyl}–C_{phenyl} plane prior to bond formation with Thr10^Y is crucial for the entropically favored binding of the ligand.

Finally, we performed a HeLa cell-based assay to investigate cell permeability of the synthesized compounds *in vivo* (Supporting Information). We obtained promising inhibition activities, thus confirming cell penetration of **5** and **6a–e**. In addition, the reversibility of the α -keto phenylamide binding mode was addressed by a dialysis experiment with **5** and the most potent inhibitor, **6a** (Supporting Information). After inhibitor treatment, the proteasome activity recurred significantly after 72 h, as expected for hemiacetal formation of the ligand with the active sites.

Discussion

Chatterjee et al.^[10b] first reported α -keto amides as P1'-extended proteasome inhibitors in 1999, yet crystallographic evaluation of the binding mode to the active site of the CP enabled detailed SAR studies only recently.^[10c] Focusing on the electronic situation of the ligand's aromatic C-terminus and its effect on binding to the CP, we plotted tabulated Hammett's constants from aromatic *para* substituents against IC₅₀ values of the synthesized α -keto phenylamides **6b–e**. We found a correlation between selected substituents of inhibitors and their biological activities, which depend on the strength of the electron donating group. Though the lead structure (**5**) was still the most active inhibitor, compared with **6b–e**, it is the polar nature of the *para*-NMe₂ or *para*-OMe groups that diminishes the biological activity. However, in contrast to nonpolar ligand interactions with lipophilic protein surfaces, the influence of hydrogen bond formation in the thermodynamic ligand binding process is more complex and still needs further experimental characterization.^[15] We thus speculate that a polar group in P1' may induce water binding and create a hydrogen bond network that entropically hinders the ligand binding process rather than stabilizes the on-target structure. By introducing methyl groups, which are nonpolar σ -donors, we were able to confirm our conclusions from the SAR studies. Subsequently, an optimal substitution pattern of methyl groups was identified by a molecular docking approach, resulting in the 2,4-dimethylated derivative **6a**. With **6a** having an IC₅₀ value of 38 nM, we could demonstrate a significant enhancement of ligand interaction and inhibitory activity relative to **5** (IC₅₀ = 72 nM). Remarkably, analysis of the crystal structure of **6a** in complex with the yeast proteasome revealed a dihedral twist of the planar conjugated π -system, which is due to increased hydrophobic interactions with the P1' binding site. This deviation from planarity stands in contrast with the rigid and planar arrangement of **5** in complex with the CP. Addressing the primed and non-primed regions of the binding channel differentiates α -keto phenylamides from the majority of known peptidic proteasome inhibitors, thus providing access to highly potent, reversible, and specific small molecule inhibitors. Furthermore, our data enable targeted ligand design in both directions of the substrate binding channel, using the α -keto phenylamide moiety as a superb linker between the primed and non-primed sites.

Conclusions

Identification and biological evaluation of the tripeptidic α -keto phenylamide **5** was the major subject of prior work, including binding mode elucidation, IC₅₀ and LD₅₀ determination, and selectivity profiling of the distinct proteasome active sites and most cytosolic serine/aspartate proteases.^[10a,c] The comparative study of different headgroup inhibitors, all bearing the Cbz-Leu-Leu-Leu-backbone, indicated ketoamide **5** as the most promising candidate to be investigated in cellular models of chemo- and immunosuppressive therapies. The aim of this study was to improve both potency and ligand efficiency of **5** while avoiding significant enlargement, as this may result in too lipophilic and thus undruggable compounds. Our SAR approach identified structure **6a** and provided improved ligand efficiency by marginal modifications of lead structure **5**. Biological evaluation of **6a** showed that the beneficial properties of the α -keto phenyl amide moiety could be conserved, while gaining improved potency against the β 5 subunit. The S1' occupation of the ligand as an additional selectivity criterion may diminish off-target side effects in humans, such as peripheral neuropathy. This disabling neuropathy is frequently observed after bortezomib treatment and even with the second generation drug carfilzomib. Furthermore, the reversible binding mode of hemiketal formation is likely to enable penetration of deeper solid tissues and allow cells to recuperate unless they are sufficiently damaged. The CP inhibitor **6a** is a promising drug candidate to address a wider range of tumor subtypes than targeted by irreversible commercial drugs, owing to its strong inhibition potency (IC₅₀ = 38 nM), and thus has emerged as a target for further investigations.

Experimental Section

Synthetic procedures

This section contains the experimental description of new compounds synthesized in this work: **6a–e**. Experimental descriptions of synthesized substrate compounds already similarly described in the literature (**8a–d**, **9a–d**) can be found in the Supporting Information. Compound **5** was synthesized by a previously published procedure.^[10a] The aldehyde substrate Cbz-Leu-Leu-Leucinal was synthesized by standardized peptide coupling from commercial enantiopure Cbz-Leu-Leu-OH and (*S*)-leucinol. Oxidation with IBX gave the desired aldehyde. IBX was synthesized following a published procedure.^[16] All chemicals that were purchased as reagent grade from commercial suppliers were used without further purification.

General methods: ¹H NMR and ¹³C NMR spectra were recorded with a Bruker AC 300 (300 MHz) or AC 500 (500 MHz) spectrometer. Chemical shifts are reported in δ (ppm), adjusted to the central line of the deuterated solvent (MeOD, CDCl₃, [D₆]DMSO). High resolution mass spectrometry (HRMS) was performed with an Agilent 1290 Infinity HPLC system coupled to an Agilent G6530A QTOF MS system. HPLC analysis was performed with an Agilent 1100 system. The purity of the final compounds was determined by UV detection (λ = 254 nm). The chromatographic method employed the following: Zorbax Eclipse XDB-C18 column, 4.6 × 150 mm; mobile phase A: H₂O (0.1% TFA), mobile phase B:

acetonitrile; flow rate: 1 mL min⁻¹; gradient elution: 30 to 100% B over 15 min. According to this method, the purities for all compounds that were evaluated in biological assays were ≥95%. Thin-layer chromatography was carried out using aluminum sheets pre-coated with silica gel 60 F254 (0.2 mm; E. Merck). Chromatographic spots were visualized by UV and/or by spraying with a methanolic solution of vanillin/H₂SO₄ or aqueous KMnO₄ solution, followed by heating. Silica gel chromatography was carried out using Merck silica gel 60 (0.063–0.2 mm).

α-Keto phenylamides (6a–e) from peptidic aldehydes and phenyl isonitriles via a Passerini reaction and subsequent oxidation of intermediate α-hydroxy phenylamides (10a–e): The peptidic aldehyde (1.0 equiv), phenyl isonitrile (1.5 equiv), and pyridine (4.0 equiv) were dissolved in dry CH₂Cl₂ (2 mL mmol⁻¹ aldehyde) and cooled to –10 °C. Trifluoroacetic acid (2.0 equiv) was added dropwise, and the reaction mixture was allowed to stir for 2 h at 0 °C. After stirring for an additional 72 h at room temperature, completion of the reaction was monitored by HPLC. CH₂Cl₂ was added, and the mixture was washed with 0.1 N aqueous HCl (3×) and aqueous saturated NaHCO₃ (3×). The organic layer was then dried over Na₂SO₄, filtered, and concentrated under reduced pressure. The resulting colorless oil and IBX (1.5 equiv) were dissolved in DMSO (2 mL mmol⁻¹ aldehyde) and stirred for 12 h at room temperature. After addition of CH₂Cl₂, the mixture was washed with water (3×), aqueous saturated NaHCO₃ (3×), and brine (3×). The organic layer was then dried over Na₂SO₄, filtered, and concentrated under reduced pressure. Purification was done via liquid chromatography.

(S)-3-(Benzyloxycarbonyl-(S)-leucyl-(S)-leucylamino)-5-methyl-2-oxo-N-(2,4-dimethylphenyl)hexanamide (6a): Yield: 21% (35 mg), colorless oil: ¹H NMR (300 MHz, CDCl₃, 300 K): δ = 8.57 (1H, s), 7.85 (1H, d, *J* = 8.7 Hz), 7.32 (5H, m), 7.05 (1H, d, *J* = 7.4 Hz), 7.01 (2H, m), 6.81 (1H, m), 5.49 (1H, m), 5.40 (1H, m), 5.08 (2H, m), 4.54 (1H, m), 4.24 (1H, m), 2.28 (3H, s), 2.24 (3H, s), 1.58 (9H, m), 0.92 ppm (18H, m); ¹³C NMR (125 MHz, CDCl₃, 300 K): δ = 196.9, 172.6, 171.9, 156.8, 156.3, 136.2, 135.6, 131.7, 131.4, 128.8, 128.7, 128.3, 128.1, 127.5, 121.8, 67.2, 53.7, 53.1, 51.7, 41.4, 40.7, 40.2, 25.4–24.8, 23.3–21.5 ppm; HPLC: *t*_R = 7.16 min, HPLC (intermediate **10a**): *t*_R = 4.98 min; HRMS calcd for [(C₃₅H₅₀N₄O₆)]Na⁺ *m/z*: 645.3627, found: 645.3629.

(S)-3-(Benzyloxycarbonyl-(S)-leucyl-(S)-leucylamino)-5-methyl-2-oxo-N-(4-*N,N*-dimethylaminophenyl)hexanamide (6b): Yield: 16% (20 mg), colorless oil: ¹H NMR (500 MHz, CDCl₃, 300 K): δ = 8.55 (1H, s), 7.50 (2H, d, *J* = 9.0 Hz), 7.33 (5H, m), 6.87 (1H, m), 6.75 (2H, m), 6.46 (1H, m), 5.39 (1H, m), 5.23 (1H, m), 5.10 (2H, m), 4.49 (1H, m), 4.18 (1H, m), 2.94 (6H, s), 1.65 (6H, m), 1.50 (3H, m), 0.90 ppm (18H, m); ¹³C NMR (125 MHz, CDCl₃, 300 K): δ = 197.0, 172.4, 171.6, 156.4, 156.3, 136.2, 128.8, 128.7, 128.4, 128.2, 121.4, 113.2, 67.4, 53.8, 53.2, 51.8, 41.4, 41.0, 40.7, 40.5, 25.4–24.9, 23.4–21.5 ppm; HPLC: *t*_R = 7.28 min, HPLC (intermediate **10b**): *t*_R = 5.91 min; HRMS calcd for [(C₃₅H₅₁N₅O₆)]H⁺ *m/z*: 638.3916, found: 638.3917.

(S)-3-(Benzyloxycarbonyl-(S)-leucyl-(S)-leucylamino)-5-methyl-2-oxo-N-(4-methoxyphenyl)hexanamide (6c): Yield: 24% (21 mg), colorless oil: ¹H NMR (500 MHz, CDCl₃, 300 K): δ = 8.26 (1H, s), 7.55 (2H, d, *J* = 9.1 Hz), 7.33 (5H, m), 6.88 (2H, d, *J* = 9.1 Hz), 6.87 (1H, m), 6.53 (1H, d, *J* = 8.2 Hz), 5.38 (1H, m), 5.29 (1H, m), 5.10 (2H, m), 4.49 (1H, m), 4.19 (1H, m), 3.79 (3H, s), 1.66 (6H, m), 1.49 (3H, m), 0.92 ppm (18H, m); ¹³C NMR (125 MHz, CDCl₃, 300 K): δ = 196.9, 172.8, 172.5, 171.8, 157.3, 156.7, 136.2, 130.0, 128.7, 128.4, 128.2, 121.6, 114.5, 67.4, 55.8, 53.8, 53.1, 51.7, 41.3, 40.7, 40.3, 25.4, 24.9, 23.4–21.3 ppm; HPLC: *t*_R = 7.89 min, HPLC (intermediate **10c**): *t*_R =

6.47 min; HRMS calcd for [(C₃₄H₄₈N₄O₇)]H⁺ *m/z*: 625.3596, found: 625.3611.

(S)-3-(Benzyloxycarbonyl-(S)-leucyl-(S)-leucylamino)-5-methyl-2-oxo-N-(4-cyanophenyl)hexanamide (6d): Yield: 12% (17 mg), colorless oil: ¹H NMR (300 MHz, CDCl₃, 300 K): δ = 8.86 (1H, s), 7.76 (2H, m), 7.65 (2H, m), 7.35 (5H, m), 6.94 (1H, m), 6.39 (1H, m), 5.28 (1H, m), 5.12 (2H, m), 4.46 (1H, m), 4.14 (1H, m), 1.73 (9H, m), 0.94 ppm (18H, m); ¹³C NMR (125 MHz, CDCl₃, 300 K): δ = 196.0, 172.6, 172.1, 157.5, 140.4, 136.0, 133.5, 128.8, 128.6, 128.2, 120.1, 118.6, 108.6, 67.5, 54.0, 52.8, 51.6, 41.1, 40.3, 39.9, 25.4–24.9, 23.3–21.6 ppm; HPLC: *t*_R = 7.75 min, HPLC (intermediate **10d**): *t*_R = 5.05 min; HRMS calcd for [(C₃₄H₄₅N₅O₆)]H⁺ *m/z*: 620.3448, found: 620.3457.

(S)-3-(Benzyloxycarbonyl-(S)-leucyl-(S)-leucylamino)-5-methyl-2-oxo-N-(4-bromophenyl)hexanamide (6e): Yield: 41% (218 mg), white solid: ¹H NMR (500 MHz, CDCl₃, 300 K): δ = 8.95 (1H, s), 7.52–7.05 (9H, m), 5.75 (1H, s), 5.29 (1H, m), 5.12–5.01 (2H, m), 4.60 (1H, m), 4.31 (1H, m), 1.57–1.26 (9H, m), 0.95–0.66 ppm (18H, m); ¹³C NMR (125 MHz, CDCl₃, 300 K): δ = 196.7, 172.4, 172.1, 157.4, 156.3, 136.2, 135.5, 132.1, 128.5, 128.2, 128.0, 121.5, 118.1, 67.1, 53.6, 53.1, 51.1, 51.4, 41.5, 40.7, 39.8, 25.2, 24.7, 23.7, 23.1, 22.8, 22.5, 22.4, 22.2, 21.4 ppm; HPLC: *t*_R = 7.68 min, HPLC (intermediate **10e**): *t*_R = 6.05 min; HRMS calcd for [(C₃₃H₄₅BrN₄O₆)]H⁺ *m/z*: 673.2595, found: 673.2605.

Biological and structural analysis

Inhibition assay of purified 20S proteasome: 100 ng of constitutive 20S proteasomes (isolated from human red blood cells) were incubated with defined concentrations of inhibitors **6a–e** for 15 min at room temperature. Equal volumes of a protease substrate solution were added (final concentration: 50 μM) and incubated at 37 °C for 1 h. Proteasome activity was recorded by the release of the fluorogenic AMC group from the protease substrate at 360 nm excitation and 460 nm emission, (LLE-AMC, VGR-AMC, and LLVY-AMC were used to analyze the different cleavage properties of the proteasome). Data, normalized to controls, represent the means of two independent experiments, each performed in triplicate (*n* = 2). Statistical analysis was performed following the methods of Cumming et al.^[17]

Intracellular inhibition of proteasomes: HeLa cells (2 × 10⁵ cells per well) were seeded in 96-well microtiter plates and cultured in RPMI supplemented with 10% FCS, 2 mM glutamine, and penicillin–streptomycin (100 U mL⁻¹ penicillin, 100 μg mL⁻¹ streptomycin). Inhibitors were added as a tenfold stock to adjust the indicated concentrations and were incubated overnight at 37 °C under 5% CO₂. The supernatant was removed, and cells were washed with cold phosphate-buffered saline and lysed in 100 μL of Tris (20 mM), EDTA (1 mM), and 0.1% NP-40. The proteasome activity was measured in 25 μL of the lysate with a final concentration of 50 μM Suc-LLVY-AMC. The assays were incubated for 1 h at 37 °C. Proteasome activity was estimated at 460 nm emission (excitation at 360 nm). Experimental data (see Supporting Information), normalized to controls, represent the means of triplicate experiments (*n* = 1). Statistical analysis was performed following the methods of Cumming et al.^[17]

Crystallization and structure determination: Crystals of the yeast CP were grown in hanging drops at 20 °C as described previously.^[1a,18] The protein concentration used for crystallization was 40 mg mL⁻¹ in Tris/HCl (20 mM, pH 7.5) and EDTA (1 mM). Drops contained 1 μL of protein and 1 μL of the reservoir solution (30 mM magnesium

acetate, 100 mM morpholino-ethane-sulfonic acid (pH 7.2), and 10% (w/v) 2-methyl-2,4-pentanediol). Crystals appeared after 2 days and were then soaked with inhibitors in DMSO at final concentrations of 2 mM for at least 24 h. Droplets were then complemented with a cryoprotecting buffer (30% (w/v) 2-methyl-2,4-pentanediol, 20 mM magnesium acetate, 100 mM morpholino-ethane-sulfonic acid, pH 6.9) and supercooled in a stream of liquid nitrogen gas at 100 K (Oxford Cryo Systems). A dataset was collected from the CP-6a complex (PDB code: 4R02) at 2.5 Å and cell parameters of $a=137$ Å, $b=301$ Å, $c=146$ Å, and $\beta=113^\circ$ in the P2₁ space group using synchrotron radiation ($\lambda=1.0$ Å) at the X06SA-beamline (Swiss Light Source, Villigen, Switzerland). X-ray intensities were assessed with the program XDS,^[19] while data reduction was carried out with XSCALE^[19] (Table ST1). Electron density was improved by averaging and back-transforming the reflections 10 times over the twofold noncrystallographic symmetry axis using the program package MAIN.^[20] Conventional crystallographic rigid body, positional, and temperature factor refinements were carried out with CNS using the yeast CP structure as a starting model (PDB code: 1RYP) (Table ST1), while model building was performed with the program MAIN.

Analysis of the reversibility of proteasome inhibition via dialysis: Red blood cell proteasome solution (500 μ L, 2 μ g proteasome) in 20 mM Tris, pH 7.2, 0.5 mM EDTA, and 0.1 mM acid (TAE) was supplemented with 25 μ L of 0.1 mM inhibitor 5 or 6a, or with 25 μ L of 1% DMSO in water. The final inhibitor concentration was 5 μ M. After pre-incubation for 30 min at room temperature, the samples were transferred to 0.5 mL dialysis tubes and dialyzed against 1 L TAE buffer at room temperature for 72 h. The buffer was exchanged after 6, 22, and 48 h. Duplicates of 25 μ L (50 ng of proteasomes) were used for estimation of activity with 100 μ M of Suc-LLVY-AMC at 460 nm emission (excitation 360 nm) at indicated time points. Experimental data (see Supporting Information) represent the means of duplicate experiments ($n=1$). Statistical analysis was laid out following Cumming et al.^[17]

Molecular docking

Preparation of protein–ligand structures: Only the $\beta 5$ and $\beta 6$ subunits of the complex were prepared; all others were removed from the system. All unbound water molecules were removed from the complexes, because they showed no significant role in ligand binding. Hydrogens were added to the X-ray structures of the CP-5 complex using the Protonate 3D function within MOE2012.10.^[14] The Protonate 3D application assigns protonation states from a discrete collection of states by optimizing the titration free energy of all titratable groups in the context of an all-atom model of a macromolecular structure (including ligands and solvent).^[21] The generalized Born/volume integral electrostatics model is used for longer range interactions and solvation effects.^[22]

Preparation of the ligand database: All five possible *ortho*- and *para*-substituted methyl-derivatives of 5 were derived from the X-ray structure by manipulation with the Builder tool of MOE. For each derivative, the dihedral angle spanning the phenyl moiety and the amide carbonyl was altered in 45° steps using the Builder software, resulting in four different conformations for each C₂-symmetrical and eight conformations for each unsymmetrical aromatic ring.

Covalent docking of the ligand database: The customized script Conflexdock was used for covalent docking of the ligands.^[23] The acetal carbon connected to Thr10^Y was assigned as the “anchor” atom and fixed in position. Conformations from the prepared data-

bases were docked into the active site and energy-minimized using the Amber12EHT force field, which is parameterized for proteins and nucleic acids using Amber and parameterized for small molecules using 2D Extended Hückel Theory.^[24] All non-anchor atoms belonging to the ligand were free to move during the minimization. The pocket atoms of the receptor were tethered to allow movement. All other atoms were fixed. To estimate the binding free energy score, the London dG scoring function was used. For visualization of the procedure, see the Supporting Information.

Supporting Information

Experimental procedures and characterization data for substrate compounds 8a–d and 9a–d; Inhibition of isolated 20S proteasomes by compounds 6a–e; Activity curves for intracellular inhibition of proteasomes by compounds 6a–e; X-ray data collection and refinement statistics; Reversibility of proteasome inhibition by compounds 5 and 6a, as determined by dialysis and proteasome activity; Molecular docking specification; NMR spectra of compounds 6a–e.

Acknowledgements

This work was supported by the Deutsche Forschungsgemeinschaft (DFG), Germany (GRK1657, projects 2E and 3C), and by the Hans und Ilse Breuer Stiftung.

Keywords: 20S proteasome · cancer · drug development · Passerini reaction · ubiquitin

- [1] a) M. Groll, L. Ditzel, J. Lowe, D. Stock, M. Bochtler, H. D. Bartunik, R. Huber, *Nature* **1997**, *386*, 463–471; b) J. Löwe, D. Stock, B. Jap, P. Zwickl, W. Baumeister, R. Huber, *Science* **1995**, *268*, 533–539.
- [2] I. Schechter, A. Berger, *Biochem. Biophys. Res. Commun.* **1967**, *27*, 157–162.
- [3] a) M. Groll, R. Huber, *Int. J. Biochem. Cell Biol.* **2003**, *35*, 606–616; b) A. K. Nussbaum, T. P. Dick, W. Keilholz, M. Schirle, S. Stevanovic, K. Dietz, W. Heinemeyer, M. Groll, D. H. Wolf, R. Huber, H. G. Rammensee, H. Schild, *Proc. Natl. Acad. Sci. USA* **1998**, *95*, 12504–12509.
- [4] A. F. Kisselev, W. A. van der Linden, H. S. Overkleef, *Chem. Biol.* **2012**, *19*, 99–115.
- [5] a) D. Chen, M. Frezza, S. Schmitt, J. Kanwar, Q. P. Dou, *Curr. Cancer Drug Targets* **2011**, *11*, 239–253; b) J. L. Thompson, *Ann. Pharmacother.* **2013**, *47*, 56–62.
- [6] A. Asai, T. Tsujita, S. V. Sharma, Y. Yamashita, S. Akinaga, M. Funakoshi, H. Kobayashi, T. Mizukami, *Biochem. Pharmacol.* **2004**, *67*, 227–234.
- [7] M. Groll, O. V. Larionov, R. Huber, A. de Meijere, *Proc. Natl. Acad. Sci. USA* **2006**, *103*, 4576–4579.
- [8] a) V. S. Korotkov, A. Ludwig, O. V. Larionov, A. V. Lygin, M. Groll, A. de Meijere, *Org. Biomol. Chem.* **2011**, *9*, 7791–7798; b) S. Kawamura, Y. Unno, A. List, A. Mizuno, M. Tanaka, T. Sasaki, M. Arisawa, A. Asai, M. Groll, S. Shuto, *J. Med. Chem.* **2013**, *56*, 3689–3700.
- [9] a) P. G. Richardson, B. Barlogie, J. Berenson, S. Singhal, S. Jagannath, D. Irwin, S. V. Rajkumar, G. Srkalovic, M. Alsina, R. Alexanian, D. Siegel, R. Z. Orlovski, D. Kuter, S. A. Limentani, S. Lee, T. Hideshima, D.-L. Esseltine, M. Kauffman, J. Adams, D. P. Schenkein, K. C. Anderson, *New Engl. J. Med.* **2003**, *348*, 2609–2617; b) M. J. Williamson, M. D. Silva, J. Terkelsen, R. Robertson, L. Yu, C. Xia, P. Hatisis, B. Bannerman, T. Babcock, Y. Cao, E. Kupperman, *Mol. Cancer Ther.* **2009**, *8*, 3234–3243.
- [10] a) H. A. Braun, S. Umbreen, M. Groll, U. Kuckelkorn, I. Mlynarczuk, M. E. Wigand, I. Drung, P.-M. Kloetzel, B. Schmidt, *J. Biol. Chem.* **2005**, *280*, 28394–28401; b) S. Chatterjee, D. Dunn, S. Mallya, M. A. Ator, *Bioorg. Med. Chem. Lett.* **1999**, *9*, 2603–2606; c) M. L. Stein, H. Cui, P. Beck, C. Dubiella, C. Voss, A. Krüger, B. Schmidt, M. Groll, *Angew. Chem. Int. Ed.* **2014**, *53*, 1679–1683; *Angew. Chem.* **2014**, *126*, 1705–1709.

- [11] K. P. Dhake, P. J. Tambade, R. S. Singhal, B. M. Bhanage, *Green Chem. Lett. Rev.* **2011**, *4*, 151–157.
- [12] R. B. Lacerda, C. K. de Lima, L. L. da Silva, N. C. Romeiro, A. L. Miranda, E. J. Barreiro, C. A. Fraga, *Bioorg. Med. Chem.* **2009**, *17*, 74–84.
- [13] a) L. P. Hammett, *J. Am. Chem. Soc.* **1937**, *59*, 96–103; b) J. Shorter, *Chem. Unserer Zeit* **1985**, *19*, 197–208; c) T. Yoshida, M. Shimizu, M. Harada, S. Hitaoka, H. Chuman, *Bioorg. Med. Chem. Lett.* **2012**, *22*, 124–128.
- [14] Molecular Operating Environment (MOE) 2012.10, Chemical Computing Group Inc., 1010 Sherbooke Street West, Suite #910, Montreal, QC, H3A 2R7 (Canada), **2012**.
- [15] H. Kubinyi in *Pharmacokinetic Optimization in Drug Research*, Helvetica Chimica Acta, Zürich, **2007**, pp. 513–524.
- [16] M. Frigerio, M. Santagostino, S. Sputore, *J. Org. Chem.* **1999**, *64*, 4537–4538.
- [17] G. Cumming, F. Fidler, D. L. Vaux, *J. Cell Biol.* **2007**, *177*, 7–11.
- [18] M. Groll, R. Huber, *Methods Enzymol.* **2005**, *398*, 329–336.
- [19] W. Kabsch, *J. Appl. Crystallogr.* **1993**, *26*, 795–800.
- [20] D. Turk, PhD thesis, Technische Universität München, **1992**.
- [21] P. Labute, *Proteins Struct. Funct. Bioinf.* **2009**, *75*, 187–205.
- [22] P. Labute, *J. Comput. Chem.* **2008**, *29*, 1693–1698.
- [23] Scientific Vector Language (SVL) source code provided by Chemical Computing Group Inc., 1010 Sherbooke Street West, Suite #910, Montreal, QC, H3A 2R7 (Canada), **2012**.
- [24] R. Salomon-Ferrer, D. A. Case, R. C. Walker, *Wiley Interdiscip. Rev. Comput. Mol. Sci.* **2013**, *3*, 198–210.

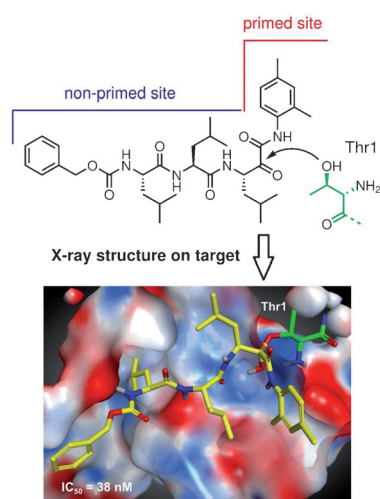
Received: June 12, 2014

Published online on ■ ■ ■■, 0000

FULL PAPERS

Prime time for proteasome inhibition:

Insights into the primed binding site of the proteasome $\beta 5$ subunit enabled targeted lead optimization for new inhibitors. Crystal structure analysis and molecular modeling allowed a structure–activity relationship study to identify a promising α -keto phenylamide-based drug candidate with unique pharmacokinetic properties.



C. Voss, C. Scholz, S. Knorr, P. Beck, M. L. Stein, A. Zall, U. Kuckelkorn, P.-M. Kloetzel, M. Groll, K. Hamacher, B. Schmidt*



α -Keto Phenylamides as P1'-Extended Proteasome Inhibitors

